Structure and dynamics of liquid selenium

F. Kirchhoff, G. Kresse,* and M. J. Gillan
Physics Department, Keele University, Staffordshire ST5 5BG, United Kingdom
(Received 30 May 1997; revised manuscript received 1 October 1997)

First-principles molecular-dynamics simulations of liquid selenium at the temperatures 570, 870, and 1370 K are presented. It is shown that calculations based on the local-density approximation are not satisfactory, because they seriously overestimate the equilibrium density of the solid and the liquid, and they give only rough agreement with measured structural data when the liquid is simulated at the experimental density. The inclusion of gradient corrections mitigates these problems, and most of the results presented are based on the generalized gradient approximation. The simulations are used to investigate the three-dimensional structure of the liquid, and results are presented for the bond-angle and dihedral-angle distributions, the concentration and structure of different Se_n rings, and the temperature-dependent length of chains. The self-diffusion constants and vibrational spectra are shown to agree satisfactorily with experimental data, and an analysis of the lifetime of covalent bonds gives insight into the diffusion mechanism. The electronic density of states of the liquid displays all the features known for the solid, and this indicates that the electronic structure changes little on melting. [S0163-1829(98)05613-6]

I. INTRODUCTION

Liquid selenium (ℓ-Se) is one of the most unusual elemental liquids, because of the twofold coordination of the atoms and the chainlike structure deduced from diffraction experiments. This unusual liquid structure is believed to be responsible for the very high viscosity just above the melting point ($T_m = 490$ K). The chain structure arises from covalent bonding between the atoms, and is closely related to the existence of a band gap and a low electrical conductivity at temperatures below the critical point ($T_c = 1860$ K, $p_c = 380$ bar).[1] This general picture of ℓ-Se has been widely accepted for many years. However, more detailed aspects of the picture are still controversial. Questions concerning the distribution of bond angles, the existence of ring structures, the length of the chains, the lifetime of the bonds, and the relation of all these to the electronic structure are still not fully resolved. In order to clarify these questions, we have performed first-principles molecular-dynamics (FPMD) simulations at three temperatures, and this paper describes the results.

Our FPMD simulations are based on density-functional theory[2] (DFT) and the pseudopotential method, following the methods pioneered by Car and Parrinello.[3] This approach is well suited to the present type of problem, since it handles the statistical-mechanical and electronic aspects in a completely unified way. DFT is generally very accurate for metals and semiconductors, and many previous FPMD simulations of liquids such as Si,[4] Ge,[5,6] V, Cu,[7] Li, Na, Al,[8,9] Ga,[10], Hg,[11] etc., have demonstrated very close agreement with experimental structural data. We have recently reported FPMD simulations of liquid Ga-Se (Ref. 12) and Ag-Se (Ref. 13) alloys at different compositions, and in the case of Ag-Se our comparisons with experimental data for the partial pair correlation functions gave evidence for the excellent realism of the simulations. There has been a previous FPMD investigation of ℓ-Se,[14] which was made at the temperature 720 K. This gave useful new insights into the structure of the liquid, but employed approximations that would not be considered necessary today. In particular, they used an empirical local pseudopotential, which was probably not as accurate as the fully *ab initio* pseudopotentials normally used now. This may account for the rather rough agreement they obtained with the measured pair-correlation function.

In fact, pure Se has special features which present a challenge to DFT. There are strong covalent bonds between neighboring atoms in the chains, but only weak bonds between atoms in different chains. DFT should be very reliable for strong bonds, but may not be so good for the weak bonds. Because of this, the question of the DFT approximation to be used is a major issue for Se. It is known from previous work[15,16] that the standard local-density approximation (LDA) used in many simulations gives a poor account of the equilibrium volume of the trigonal Se crystal (*t*-Se), precisely because of the weak-bond problem. The inclusion of gradient corrections (GC) using a generalized gradient approximation[17] (GGA) gives a much better description of *t*-Se.[15,16] We have therefore paid special attention to the comparison of LDA and GGA in the present work, and we shall show that GC give a substantial improvement.

The average twofold coordination in ℓ-Se has been firmly established by structural investigations using neutron[18–21] and x-ray[22] diffraction and measurements of extended x-ray-absorption fine structure,[23] and these experiments have shown that the coordination remains close to 2 up to the critical point. However, since these experiments probe only pair correlations, they cannot give direct information about the three-dimensional liquid structure. Some information about typical bond angles can be inferred from the peaks in the pair-correlation function, but a true bond-angle distribution cannot be deduced. Information about the dihedral-angle distribution in the chains is even harder to glean, and models such as the ''free-rotating-chain model''[21,24] are only weakly constrained by experimental data. Controversies about the existence or absence of ring structures[24–26] are equally difficult to settle. The simulation results presented here give di-

rect information about these questions of three-dimensional structure.

The high viscosity of ℓ-Se at just above T_m (Ref. 27) is one of the important pieces of evidence for the existence of long chains in the liquid. The viscosity drops rapidly with increasing T, and at $T \simeq 1000$ K it is similar to that of normal liquid metals like Na;[27] this suggests that the chain length also drops rapidly. Our simulations give direct evidence for this decrease of chain length, but we shall emphasize that estimates of chain length depend heavily on how the length is defined. This question is related to the existence of defects in the liquid, as shown for example by the experimental work of Warren and Dupree,[28] who used nuclear magnetic resonance to determine the concentration of chain ends. The analysis of the present FPMD calculations to study the nature of the defects in the liquid will be presented in a separate paper.[29] The calculations described here have been used to study the self-diffusion constant D, which is indirectly related to the viscosity. We shall show that our D values agree semiquantitatively with experimental data, and that they increase rapidly with temperature, as would be expected from the decrease of viscosity. We also investigate the bond lifetime, and show that its relation to D sheds light on the diffusion mechanism. Further information about the dynamics of the atoms is given by the vibrational spectrum, and we shall see that the spectrum of the simulated system agrees closely with that obtained by neutron scattering.

Finally, our simulations will be used to study the electronic density of states (DOS) of ℓ-Se. This will give strong evidence that the electronic structure of the liquid is essentially the same as that of the solid, at least in the temperature range we have covered. However, there are difficulties in comparing the DOS directly with experimental data, because our present calculations yield only Kohn-Sham single-particle energies, rather than the quasiparticle energies probed experimentally.

The plan of the paper is as follows. Section II outlines the methodology of the simulations. A detailed comparison between calculations based on LDA and GGA, both for t-Se and for ℓ-Se at 870 K, is presented in Sec. III. The comparison of our calculated structural data with experiment, and our analysis of the three-dimensional structure are presented in Sec. IV, and our results for the self-diffusion constants, the vibrational spectra, and the bond lifetime are given in Sec. V. In Sec. VI, we report our results for the electronic structure. The paper concludes with a summary of our conclusions (Sec. VII). We note that a Brief Report of some of the present results has already been published.[30]

II. METHODOLOGY

The general principles of the DFT-pseudopotential methods used in our static and dynamical calculations have been thoroughly described in reviews,[31] and we mention here only the features relevant to the present work. All the calculations were done with VASP (Vienna *ab initio* simulation package).[32,33] In VASP, the ground state for each set of ionic positions is calculated using an efficient iterative matrix-diagonalization scheme and a Pulay mixer.[34] A smearing method is used to avoid problems with level crossing,[35,36] and the free energy is used as the variational quantity. Further details of the computational method can be found in Refs. 32,33. In the dynamical simulations, convergence to the ground state at each time step is accelerated by extrapolating the wave functions and the charge density from previous steps, as described in Ref. 6. This extrapolation guarantees that only about three or four electronic iterations are needed to determine the electronic ground state to an accuracy of 10^{-5} eV/atom.

As usual in the DFT-pseudopotential method, the valence orbitals are expanded in a plane-wave basis characterized by a plane-wave cutoff energy $E_{\rm cut}$. We use pseudopotentials of the ultrasoft Vanderbilt type,[37,38] which have the advantage that very high accuracy is achieved with rather modest values of $E_{\rm cut}$ (i.e., rather small basis sets). The ultrasoft pseudopotentials for Se were constructed with a scheme[38] similar to the one proposed by Rappe *et al.*[39] Two energy channels were used for the s and p wave functions, and the cutoff radii for the wave functions and the augmentation charges[38] were set to 2.5 and 2.2 a.u., respectively. A norm-conserving d pseudopotential was chosen as the local pseudopotential. Nonlinear partial-core corrections were included in the pseudopotentials.[40] This construction scheme results in an excellent description of the scattering properties: logarithmic derivatives for all-electron and pseudowave functions are virtually indistinguishable over an energy range of 4 Ry.

An important feature of the present work is that we have employed both the local-density approximation (LDA) and the generalized gradient approximation (GGA). Our LDA calculations use the exchange-correlation function of Ceperley and Alder,[41] and our GGA calculations use the PW91 functional due to Perdew and Wang.[17] The GGA was used consistently for the generation of the pseudopotential and the calculations on solid and liquid Se.

Our dynamical simulations of the liquid use Γ-point sampling and a plane-wave cutoff of 150 eV. With the ultrasoft pseudopotentials we use, this cutoff gives an error in the total energy of less than 10 meV/atom, so that all results are very well converged with respect to the size of basis set. The dynamical simulations were all done on a system of 69 atoms in the canonical ensemble using a Nosé thermostat,[42] with a time step of 3 fs. The energy conservation was excellent for all runs: as an example, we found that at 870 K the drift was smaller then 0.5 meV/atom/ps. The density of the liquid was set equal to the experimental value.

III. THE EFFECT OF THE GRADIENT CORRECTIONS

A. The trigonal Se crystal

We investigated the effect of GC on crystalline Se in preparation for our work on the liquid. The question of GC effects in solid Se has been discussed before (see Refs. 15,16), but we needed to reexamine it because the pseudopotentials used here differ from those used before.

The most stable structure of crystalline Se is the trigonal phase t-Se. This structure has a hexagonal Bravais lattice with three atoms per unit cell, and is characterized by infinite helical chains parallel to the c axis, with three atoms per turn. In addition to a and c, one usually defines a third structural parameter u, which is the radius of the helix in units of

TABLE I. Calculated equilibrium structural parameters (volume per atom Ω, c/a ratio, internal parameter u, bond angle Θ, intrachain distance d_1, interchain distance d_2, second-nearest-neighbor intrachain distance d_3, and bulk modulus B) of t-Se compared to experiment and to previous calculations. LDA refers to local-density calculations, GGA to calculations with the generalized gradient approximation, NC to calculations using norm-conserving pseudopotentials, and US to calculations using ultrasoft pseudopotentials.

	Ω (Å^3)	c/a	u	Θ (deg)	d_1 (Å)	d_2 (Å)	d_3 (Å)	B (GPa)
LDA-US[a]	23.24	1.30	0.258	103.1	2.46	3.10		30.5
LDA-NC[b]	22.94	1.30	0.256	103.4	2.44	3.09		
LDA-NC[c]	24.79	1.21	0.243	103.2	2.42	3.23		16.8
LDA-NC[d]	22.43	1.24	0.248	102.8	2.37	3.10		
GGA-US[a]	28.77	1.16	0.226	103.8	2.43	3.49	3.82	7.1
GGA-NC[b]	28.63	1.18	0.224	105.7	2.42	3.49		
Expt.[e]	27.26	1.136	0.2246	103.3	2.37	3.44	3.72	14.9

[a]Present work.
[b]Reference 15.
[c]Reference 44.
[d]Reference 45.
[e]Reference 43.

a. The internal parameter u defines the position of the atoms in the unit cell as $(u,0,0)$, $(0,u,1/3)$, $(\overline{u},\overline{u},2/3)$ in units of the lattice vectors.

In Table I we report our results for the equilibrium structural parameters of t-Se, together with a comparison with experiment[43] and other theoretical studies[44,45] (calculation details like k-point samplings are the same as in Ref. 16). In spite of the difference of pseudopotentials, our calculated structural properties are virtually identical to those of Ref. 16, and the latter results are not shown. It can be seen that LDA underestimates the volume by almost 15%, whereas GGA gives much better agreement with experiment. As often happens, the GC have a tendency to over correct, but for Se the overestimation of volume is a fairly modest 5%.

It might seem at first sight that GGA also improves the overall agreement of other structural parameters like c/a and u, but this is in fact not the case. The GC change neither the electronic density of states (DOS) nor the bonding properties significantly for a *fixed* volume. This was demonstrated in Ref. 16 by showing that the structures predicted by LDA and the gradient corrected schemes for a set of fixed volumes are virtually identical. To further confirm this point, and to probe the nature of the local bonding, we calculated two zone-center phonon frequencies. The $\Gamma_1(A_1)$ phonon corresponds to a breathing mode of the chains, i.e., to a mode in which the radius of the chains varies. Both the strong intra- and weak interchain bonds contribute to this mode. To probe the weak interchain bonding alone, we considered a second phonon mode $\Gamma_2(A_2)$, in which the chains rotate *rigidly* leaving the intrachain bonds inert. The phonon frequencies were calculated using a simple frozen-phonon approach, in which the total energy was calculated for a series of displacements. A cubic fit to these results was performed to give the second derivatives of the energy with respect to the displacements. We calculated the phonon frequencies for both the theoretical and the experimental lattice constants; the final results with a comparison to experiment[46,47] are shown in Table II. At the experimental lattice constants the phonon frequencies calculated with the LDA and GGA are only marginally different, which confirms that the GC do not change the local bonding properties for a fixed volume. The overall agreement of the GGA results with experiment is satisfactory, whereas LDA results at the theoretical LDA volume are wrong by more than 20%.

B. Liquid Se at 870 K

The calculations presented in the previous section demonstrate that the equilibrium volume of trigonal selenium can be improved substantially by the addition of GC to the LDA. We will now show that inclusion of GC is even more important in the liquid phase. We have done FPMD simulations at the temperature 870 K using both LDA and GGA, both simulations being performed at the experimental density.[48,49] Details of these simulations are given in Table III. (The table also contains details of our other simulations at 570 and 1370 K, which will be discussed in Sec. IV.)

In Figs. 1 and 2 we show our results for the static structure factor $S(k)$ and the pair-correlation function $g(r)$ for the LDA and the GGA simulations at 870 K, and compare them with experimental data. The most direct comparison between theory and experiment is via the static structure factor defined as

TABLE II. Frequencies (in units of cm^{-1}) of the $\Gamma_1(A_1)$ and $\Gamma_2(A_2)$ zone-center phonons of t-Se compared to experimental values. The frequencies have been calculated for the theoretical LDA, respectively, GGA lattice parameters and for the experimental lattice parameters (in parentheses). We also show the LDA result of Ref. 45 for comparison.

	$\Gamma_1(A_1)$	$\Gamma_2(A_2)$
LDA-US	177.8 (217.5)	136.0 (93.3)
GGA-US	217.6 (213.9)	94.5 (91.8)
LDA-NC[a]	206	
Expt.	237[b]	102[c]

[a]Reference 45.
[b]Reference 46.
[c]Reference 47.

TABLE III. Temperature T, density ρ, and number density n at which simulations were done (experimental densities were taken from Refs. 48,49). Also shown is the experimental pressure P_{exp}, the length of the equilibration t_{equ}, and the length of the simulation t over which properties were sampled.

T(K)	ρ (g/cm^3)	n (Å^{-3})	P_{exp} (bars)	t_{equ} (ps)	t (ps)
570	3.91	0.0298	1	5	10
870	3.57	0.0272	10	5	18
1370	3.08	0.0238	100	3	7

$$S(k)=\langle|\hat{\rho}_{\mathbf{k}}|^2\rangle, \tag{1}$$

where $\hat{\rho}_{\mathbf{k}}$ is the dynamical variable representing the density of atoms at wave vector $\mathbf{k}$:

$$\hat{\rho}_{\mathbf{k}}=N^{-1/2}\sum_{i=1}^{N}\exp(i\mathbf{k}\cdot\mathbf{R}_i). \tag{2}$$

Here, the sum goes over all N atoms in the system. We have calculated $S(k)$ directly from this formula for $\mathbf{k}$ vectors commensurate with the periodic boundary conditions. The overall agreement of $S(k)$ with experiment is reasonable for both LDA and GGA, but the GGA shows much better agreement, especially in the range of the first peak. In the experimental structure factor, one sees that the first peak at 4 Å^{-1} has a distinct shoulder around 2 Å^{-1}, which is well reproduced by the GGA calculation. The LDA calculation shows only a broad maximum around 3 Å^{-1}. Even more worrying is the behavior of the LDA structure factor at low wave vectors, where it appears to be tending to a large value as $k\rightarrow 0$, whereas the GGA $S(k)$ remains in good agreement with experiment in this region.

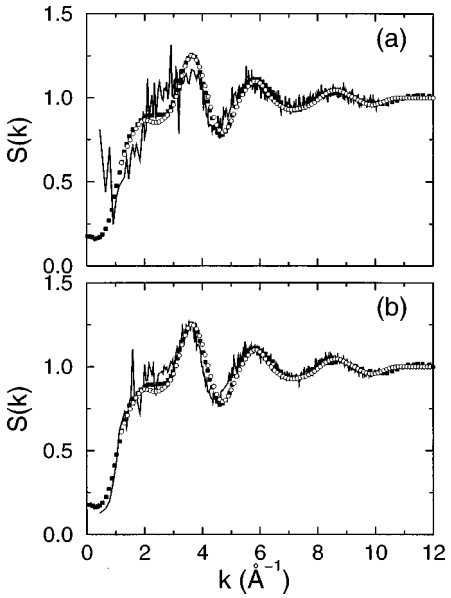

FIG. 1. The static structure factor $S(k)$ of liquid Se at 870 K from LDA (a) and GGA (b) simulations (continuous curves), compared with experimental results from neutron scattering (Ref. 21) (filled squares) and x-ray diffraction (Ref. 22) (open circles).

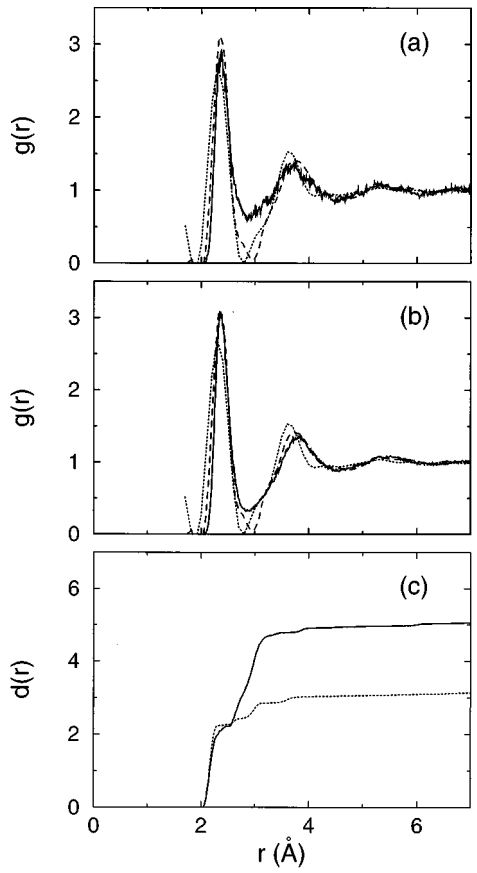

FIG. 2. The pair-correlation function $g(r)$ of liquid Se at 870 K from LDA (a) and GGA (b) simulations (continuous curves), compared with experimental results from neutron scattering (Ref. 21) (dashed curves) and x-ray diffraction (Ref. 22) (dotted curves). Panel (c) shows the function $d(r)$ characterizing the difference between simulated and experimental $g(r)$ (see text) for LDA (continuous curve) and GGA (dotted curve).

In order to understand the anomalous behavior of the LDA $S(k)$ at small k, we need to note that $S(k\rightarrow 0)$ is related to the isothermal compressibility κ_T by the equation:[50]

$$\lim_{k\rightarrow 0}S(k)=nk_BT\kappa_T, \tag{3}$$

where n is the number density and k_B is Boltzmann's constant. A large value of $S(k\rightarrow 0)$ therefore indicates a highly compressible liquid. It seems fairly clear that this is closely related to the serious underestimation of the equilibrium volume by LDA in t-Se. Since the liquid simulations were performed at the experimental density, we would expect LDA to give a pressure that is too low. To check this, we have calculated the pressure over a short part of the simulation, and we find a value of -3 kbars, so that the liquid is actually under tension. We would expect the liquid to be more compressible under tension, and this would explain the high LDA value of $S(k\rightarrow 0)$.

There are signs that the liquid simulated with LDA may be verging on instability. If a liquid is expanded, the compressibility diverges on the spinodal line, the intensity of long-wavelength density fluctuations becomes unbounded, and internal surfaces are created. We have found that snapshots of instantaneous configurations do indeed show large

TABLE IV. The positions $r^{(1)}_{max}$, $r^{(1)}_{min}$, and $r^{(2)}_{max}$ of the first maximum, first minimum, and second maximum (Å units) of the pair-correlation function $g(r)$, and the values of $g(r)$ at these positions, obtained from the present LDA and GGA simulations, compared with experimental data from neutron (Ref. 21) and x-ray (Ref. 22) diffraction.

	$r^{(1)}_{max}$	$r^{(1)}_{min}$	$r^{(2)}_{max}$	$g(r^{(1)}_{max})$	$g(r^{(1)}_{min})$	$g(r^{(2)}_{max})$
LDA	2.37	2.88	3.71	2.9	0.6	1.3
GGA	2.37	2.88	3.83	3.1	0.3	1.35
Neutron	2.36	2.95	3.74	3.1	0.0	1.4
X-ray	2.32	2.8	3.60	2.7	0.0	1.5

density fluctuations and suggest the incipient formation of internal surfaces. Clearly, simulations at the experimental volume can be dangerous and misleading if the approximations being used fail to describe the experimental equilibrium volume correctly. In concluding this discussion of $S(k)$, we stress again that the GGA gives a good account of $S(k)$ and does not suffer from the serious problems encountered by the LDA.

In Fig. 2 the pair-correlation functions $g(r)$ from our LDA and GGA simulations are compared with experimental data. To provide more quantitative information, we give in Table IV numerical values for the positions $r^{(1)}_{max}$ and $r^{(2)}_{max}$ of the first and second maxima and the position $r^{(1)}_{min}$ of the first minimum, and values of $g(r)$ at these positions. We note that comparison of the pair-correlation function with experiment can be problematic, because of the well-known difficulties of Fourier transforming the experimentally determined structure factor. The experimental $g(r)$ data from neutron[21] and x-ray[22] diffraction differ significantly from one another, whereas the corresponding structure factors agree well. The comparisons presented in Fig. 2 and Table IV show that the LDA and GGA simulations reproduce rather well the position and height of the first maximum. Both LDA and GGA also give fairly good accord with experiment for the position and height of the second maximum, though we note the significant disagreement between the x-ray and neutron results in this region. However, there is a substantial difference between LDA and GGA around the first minimum. The main shortcoming of our LDA calculations is that the depth of the first minimum in $g(r)$ is seriously underestimated—a problem also encountered by Hohl *et al.*[14] in their LDA-based FPMD simulations. Our GGA calculations, by contrast, give a first minimum in much better agreement with experiment, though there is still some discrepancy.

In order to provide a quantitative measure of the structural improvement given by GGA, we have calculated the following quantity characterizing the difference between the simulated and experimental $g(r)$:

$$d(r)=\left[4\pi n\int_0^r dr' r'^2 |g_{sim}(r')-g_{exp}(r')|^2\right]^{1/2}. \quad (4)$$

The bottom panel of Fig. 2 compares the $d(r)$ calculated with the simulated pair-correlation functions $g_{sim}(r)$ obtained from LDA and GGA; the experimental function $g_{exp}(r)$ is taken from the neutron-diffraction data.[21] The $d(r)$ values demonstrate that the LDA and GGA $g(r)$ are almost identical for r values up to the first maximum. However, for larger r values, and particularly in the region of the first minimum, GGA produces a very marked reduction in $d(r)$ compared with LDA, and this demonstrates the quantitative superiority of GGA.

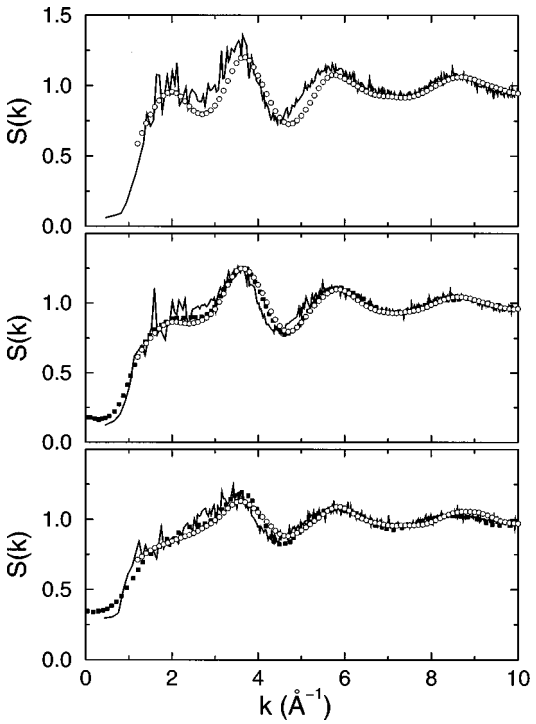

FIG. 3. The static structure factor $S(k)$ of ℓ-Se from GGA simulations (continuous curves) at 570 (top), 870 (middle), and 1370 K (bottom) compared with experimental results from neutron scattering (Ref. 21) at 870 K, 15 bars and 1373 K, 75 bars (filled squares) and x-ray diffraction (Ref. 22) at 573 K, 12 bars, 873 K, 16 bars, and 1473 K, 120 bars (open circles).

IV. STATIC STRUCTURAL PROPERTIES OF ℓ-Se

A. Structure factor and pair-correlation function

We now move on to the comparison of the structural properties of ℓ-Se at the three simulated temperatures. From now on, we will be concerned only with simulations based on GGA, and a summary of our simulations (including the one at 870 K already discussed) is given in Table III. Results for the static structure factor and a comparison with available experimental data are shown in Fig. 3. At the two higher temperatures the agreement with experiment is good, but the agreement is less good at the lowest temperature. For all three temperatures, both the large-k behavior and the small-k behavior are almost perfect, though for large k one can see a small inward shift of the theoretical results compared with experiment. The agreement in the intermediate k regime is less satisfactory. For all three temperatures, the minimum in $S(k)$ around 5 Å^{-1} is shifted inward. For the lowest temperature, the first peak $S(k)$ is more pronounced than in the experiment and it is also shifted towards smaller k values.

The pair-correlation function $g(r)$ is compared with experimental results in Fig. 4, and the positions r_{max} and r_{min} of the first maximum and first minimum of $g(r)$ according to

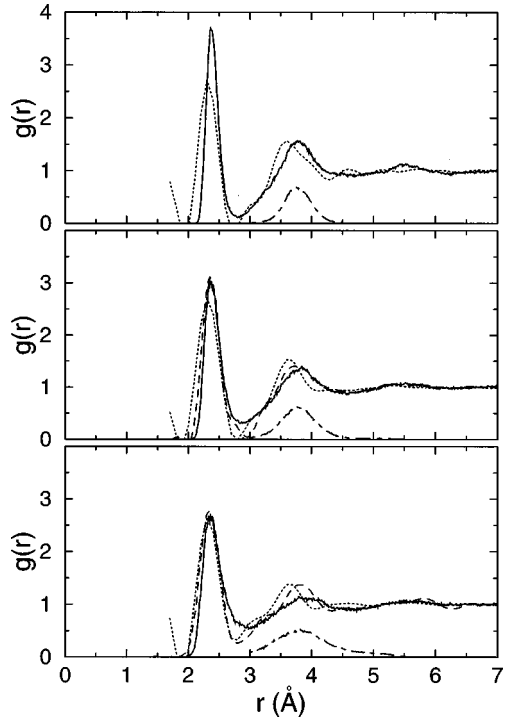

FIG. 4. The pair-correlation function $g(r)$ of liquid Se from GGA simulations (continuous curves) at 570 (top), 870 (middle), and 1370 K (bottom), compared with experimental results from neutron scattering (Ref. 21) at 870 K, 15 bar and 1373 K, 75 bars (dashed curves) and x-ray diffraction (Ref. 22) at 573 K, 12 bars, 873 K, 16 bars, and 1473 K, 120 bars (dotted curves). Also shown is the pair correlation between second neighbors $g^{\text{second}}(r)$ (chain curves, see text).

our simulations are reported in Table V. We note once again that the comparison with experimental pair-correlation functions is problematic. Among the experiments, the real-space resolution of the neutron-diffraction data is best, because $S(k)$ was measured up to 15 Å^{-1},[21] whereas the k range in the x-ray-diffraction experiment was more limited (from ~ 1 Å^{-1} to ~ 10 Å^{-1}).[22] Overall, the position and the height of the first peak in our results agree very well with neutron data. We note however that the first peak is shifted slightly outward in comparison with experiment, which is consistent with the inward shift of $S(k)$ for large k in comparison with experiment. It is relevant to recall that the first three-neighbor distances in the solid phase are also overestimated by 1.5–2 % (see Table I).

More problematic, however, is the behavior around the first minimum r_{min} in the pair-correlation function. For the two lower temperatures, all experimental curves drop almost to zero around the first minimum. The gradient corrections improve the behavior around r_{min} but some discrepancies remain. In addition, the second peak seems to be shifted outward compared with the x-ray experiments, though it can be seen that both the x-ray and neutron data show spurious oscillations around the first minimum and the second peak, so that it is rather difficult to assess this point accurately. In discussions of ℓ-Se it is usually assumed that the second peak in $g(r)$ is associated with the second-neighbor distance *within* a chain. This is suggested by the fact that in the solid the second-neighbor intrachain distance (d_3) is very similar to the position of the second peak in the liquid state $g(r)$ (see Table I). We have tried to confirm this viewpoint by calculating the pair-correlation function between second nearest neighbors $g^{\text{second}}(r)$ within one chain. For this calculation we have defined nearest neighbors as atoms for which the bond length is smaller than r_{min}. Our results are also shown in Fig 4. One can see that $g^{\text{second}}(r)$ accounts almost entirely for the position and general magnitude of the second peak, confirming the experimental point of view.

TABLE V. Position of the first maximum r_{max} and first minimum r_{min} in $g(r)$ and the coordination numbers N_c^{fix} and N_c^{min} obtained by integrating the radial distribution function up to $r_c = 2.82$ Å and $r_c = r_{\text{min}}$, respectively. Also shown fraction f_2 of twofold-coordinated sites, the average nearest-neighbor distance $\langle r \rangle$, the average bond angle $\langle \Theta \rangle$, and their root-mean-square deviation.

T(K)	r_{max} (Å)	r_{min} (Å)	N_c^{fix}	N_c^{min}	f_2	$\langle r \rangle$ (Å)	$\langle \Theta \rangle$ (deg)
570	2.38	2.82	2.00	2.00	0.95	2.42±0.11	104±10
870	2.37	2.88	2.00	2.06	0.88	2.44±0.14	105±14
1370	2.36	3.00	1.88	2.16	0.71	2.45±0.17	107±19

We note from Table V that the position r_{max} of the first maximum of $g(r)$ varies hardly at all with temperature, while the first minimum r_{min} moves outward by almost 0.2 Å as T goes from 570 to 1370 K.

B. Coordination number

There has been considerable debate in the literature about the temperature dependence of the coordination number N_c in ℓ-Se, i.e., the average number of first neighbors surrounding any atom. It should be recognized that this is not a precisely defined quantity, because it depends on the cutoff distance r_c used to define what counts as a first neighbor. A common procedure is to take r_c equal to the position of the first minimum r_{min}, which implies that r_c varies with temperature. We denote the coordination number defined in this way by N_c^{min}. An alternative definition is to assign a fixed temperature-independent value to r_c, and we denote the corresponding coordination number by N_c^{fix}. We have calculated N_c in both ways, taking the value $r_c = 2.82$ Å for N_c^{fix}, and the results are reported in Table V. At the lowest temperature, N_c is exactly equal to 2, as expected from the conventional picture of low-temperature ℓ-Se consisting of long chains, as in t-Se. Broadly, N_c remains fairly close to 2 up to 1370 K, but in detail the answer to whether N_c increases or decreases depends on the exact definition adopted. The fact that N_c^{min} increases with temperature (see Table V) is not surprising, since we have seen already that r_{min} moves outward with temperature.

Also shown in Table V is the average first-neighbor distance $\langle r \rangle$ defined by

$$\langle r \rangle = \int_0^{r_c} r g(r) r^2 dr \Big/ \int_0^{r_c} g(r) r^2 dr, \tag{5}$$

which we calculate with the fixed r_c equal to 2.82 Å. Our results show that $\langle r \rangle$ increases slightly with T in spite of the slight decrease of r_{max}. This effect is due to the increasing

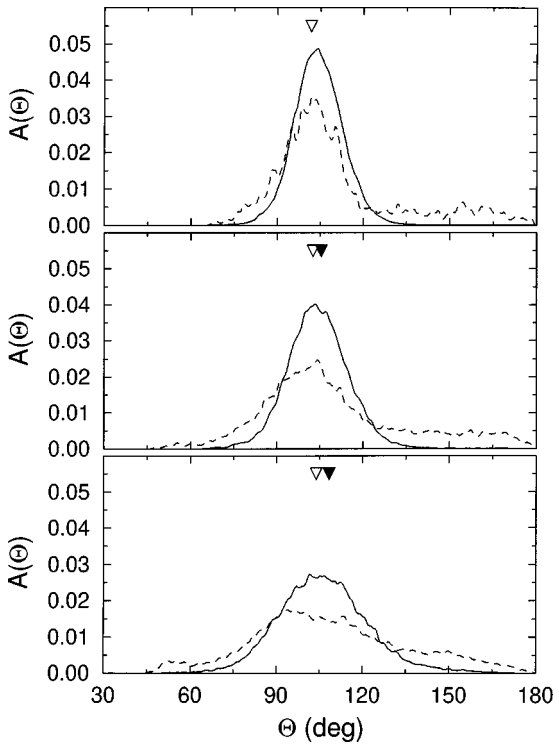

FIG. 5. The bond-angle distribution $A(\Theta)$ of ℓ-Se at 570 (top), 870 (middle), and 1370 K (bottom) for twofold-coordinated atoms (continuous lines) and threefold-coordinated atoms (dashed lines). All distributions have been normalized to unity. The average bond angles extracted from x-ray (Ref. 22) and neutron-scattering (Ref. 21) are shown as white and black triangles, respectively.

asymmetry of $g(r)$ as T is raised. Unfortunately, none of the experiments had a real-space resolution sufficient to resolve this asymmetry.

Finally, we note the values given in Table V for the percentage of atoms which are twofold coordinated (results are the same for both sets of r_c). As expected, nearly all atoms are twofold coordinated at 570 K, but the percentage is strongly reduced to $\sim$ 70% at 1370 K. An important way of pursuing further the question of deviations from twofold coordination is in terms of defects, as has been done in earlier work.[14] A full discussion of defects in ℓ-Se will be given in a separate paper.[29]

C. Three- and four-body correlation functions

So far we have studied the structure of ℓ-Se using quantities that are also accessible to experiments. However, the limited information available in two-body correlations is insufficient to understand the structure of a molecular liquid like ℓ-Se. We now present results for the bond-angle and dihedral-angle distributions, which give three- and four-body information. The nearest-neighbor cutoff distance r_c needed to define these distributions is taken to be the first-minimum distance $r_{\min}$, but in fact we have verified that the results are scarcely affected if we take a fixed value of r_c.

The bond angle distribution $A(\Theta)$ is shown in Fig. 5 for 570, 870, and 1370 K. In addition to calculating $A(\Theta)$ itself, we have also obtained the partial contributions $A_2(\Theta)$ and $A_3(\Theta)$ from atoms which are twofold and threefold coordinated, and these distributions are also shown in Fig. 5. At all three temperatures the bond-angle distribution is dominated by the $A_2(\Theta)$ contribution, and shows a sharp symmetric peak in the region of 104°. The fact that $A_2(\Theta)$ is narrow reflects the highly directional character of the strong covalent bonds between nearest neighbors within chains. The main noticeable effect of the increasing temperature is to broaden $A_2(\Theta)$, with the root-mean-square deviation of the bond angle increasing from 10° to 20° (detailed values are given in Table V).

The average bond angles found in our simulation are essentially identical to the bond angle found in the helical chains of t-Se (see Table I). In addition it is possible to estimate the average bond angle Θ from the results of diffraction experiments, if the first and second peaks in $g(r)$ are associated with the average first and second intrachain neighbor distance, respectively. The values for the bond angle derived from neutron-scattering[21] and x-ray diffraction[22] in this way are also in good agreement with our findings (see Fig. 5). The experimental results suggest that there is an increase in the average bond angle with temperature, which is confirmed by our simulation (see Table V). The increase in the average bond angle is partly due to an increase of the bond angle for the twofold-coordinated atoms, and partly due to an increase of the fraction of threefold-coordinated atoms, for which we find an average bond angle around 109° (see Fig. 5).

Interestingly, the bond-angle distribution $A_3(\Theta)$ has a fairly sharp maximum roughly in the same region as $A_2(\Theta)$, but there is a nonvanishing fraction of atoms with bond angles up to 180°. This has an interesting interpretation. We have found that threefold-coordinated atoms are usually characterized by two short bonds and one long one. The bond-angle distribution for the two shorter bonds is almost identical to the one for twofold atoms, whereas the third (long) bond shows a random distribution, and accounts for most of the differences between $A_3(\Theta)$ and $A_2(\Theta)$. This is a clear indication that Se atoms strongly favor twofold coordination: if a third neighbor approaches, its bonding will be weak, with no strong preference for a particular bond angle.

We now turn to four-body correlations, which are conveniently characterized by the dihedral-angle distribution $D(\gamma)$ shown in Fig. 6. We see that the distribution is nonvanishing from 0° to 180°, showing that the dihedral angle γ can assume all values in this range. At 570 K, $D(\gamma)$ exhibits a clear maximum around $\gamma \sim 90°$. From calculations on small isolated H_2Se_2 (Ref. 51) and Se_4 (Ref. 52) molecules, this value of γ is known to be energetically favored, because of repulsion between lone-pairs on neighboring atoms. In addition, the crystal structures of Se are characterized by a dihedral angle around 90°. The preference for these dihedral angles clearly persists in the liquid. At 870 K the distribution of the dihedral-angle distribution flattens, with a visible increase in the fraction of planar conformations with $\gamma \sim 0°$ or $\gamma \sim 180°$. In addition the maximum of $D(\gamma)$ has shifted to a smaller value around $\gamma \sim 80°$. This shift in the maximum may possibly be connected with the presence of rings in the liquid, as discussed later (see Sec. IV E). Finally at 1370 K, $D(\gamma)$ becomes quite structureless.

Since the dihedral angle cannot be determined directly from experiment, there has been considerable controversy

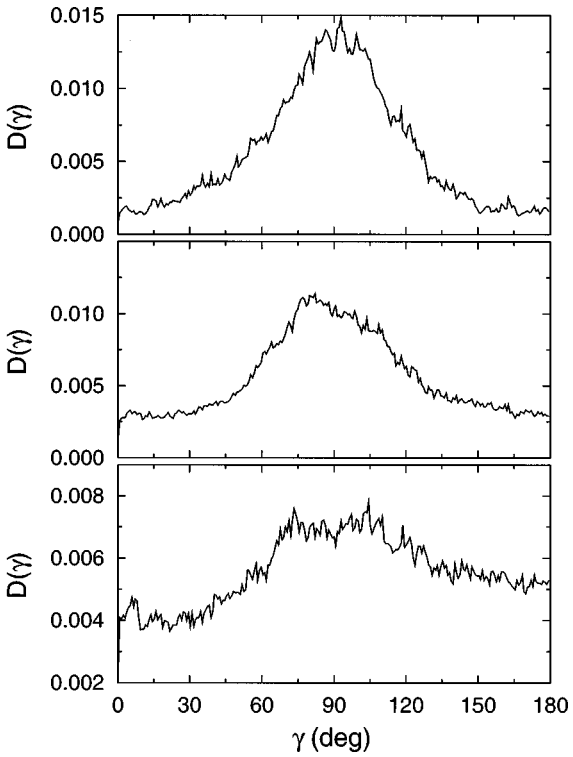

FIG. 6. The dihedral-angle distribution $D(\gamma)$ of ℓ-Se at 570 (top), 870 (middle), and 1370 K (bottom). All distributions have been normalized to unity. Note the different scale for the highest temperature.

about the possible values of γ in ℓ-Se. Several models have been proposed in the literature to understand the structure of a-Se and ℓ-Se (many of these models are discussed in Ref. 14). The controversy stems largely from the fact that the dihedral angle affects the two-body correlations only at the fourth-neighbor level, which means that several different models may be consistent with the same pair-correlation function. Several authors showed that the so-called nearly free rotating chains model,[21,24] which assumes rigid bond lengths and angles but randomly distributed dihedral angles, can reproduce the measured pair-correlation function of ℓ-Se very well.[21,24] Our results indicate that this model is incorrect at low temperatures, since $D(\gamma)$ is markedly nonuniform in this region. We also note that this is in contrast to the results of the tight-binding simulations of Bichara *et al.*[53] who found that $D(\gamma)$ is essentially uniform.

D. Chain length

The majority of atoms are twofold coordinated at all temperatures, and it is natural to estimate the average length of chains. In order to make a rough estimate, we define a chain as a sequence of twofold coordinated atoms ending in either a one- or threefold-coordinated atom. We must stress that this is only one possible definition. Indeed, it is not at all obvious that a definition based on coordination numbers alone has any close connection with the experimental measurements that have often been used to deduce chain lengths. This is a complex matter which is intimately linked with the question of defects in the liquid, and will be discussed in depth elsewhere.[29]

With our simple geometrical definition, we obtain average chain lengths of 25, 12, and 5 at 570, 870, and 1370 K. These figures clearly indicate that the average chain length decreases with temperature, but the absolute values should not be taken too seriously. In addition to the problems connected with a purely geometrical definition, one can also question whether our MD runs, long though they are, are really long enough to estimate reliable chain lengths at low temperatures. Although we have done a long equilibration for each temperature, we found that the average chain length at 870 K increases during the simulation from 10 to 14, indicating that the run may not be completely converged in this respect. The 570 K system is even worse because it shows only very slow diffusion (see Sec. V).

E. Ring size

Because the presence of rings in ℓ-Se has often been debated in the past,[26] we have done a careful ring analysis of our simulations. We define a ring as a closed loop of atoms, containing at most one threefold or fourfold atom. This definition includes isolated rings but also allows for loops having one bond to another chain or ring. Because of the periodic boundary conditions, large closed chains with sizes exceeding the unit cell can occur. To eliminate these exceptions we define the dimension of the loops as the largest distance between two atoms within the chain. If this dimension exceeds the size of the unit cell, the loop is classified as a chain, otherwise as a ring.

A significant concentration of rings was only found for 870 K, whereas no rings were observed at 570 K, and only a negligible number at 1370 K. Even at 870 K, the concentration of rings was small: the average numbers of Se_6 and Se_7 rings in the entire 69-atom system were 0.4 and 0.5, respectively, the concentrations of other types of rings being negligible. The Se_6 and Se_7 rings we found in the simulation were well defined and usually formed by twofold-coordinated atoms only. Especially the Se_7 rings showed remarkable stability, and two well-defined rings remained stable for more than 6 ps. The absence of rings at low temperature may indicate that chains have a lower free energy than rings; their very small concentration at high temperatures is presumably due to the fairly high concentration of onefold and threefold atoms.

Because Se_8 and Se_6 rings occur in the monoclinic[54] and the rhombohedral phase[55] respectively, is was long believed that there might be a large concentration of similar rings in ℓ-Se and in a-Se.[26] Our simulations show that the fraction of Se_8 rings is only very small. This is very similar to the situation found in the vapor phase at similar temperatures, where Se_5, Se_6, and Se_7 predominate, with only traces of Se_8.[56]

The typical configurations for Se_6 and Se_7 rings found in the liquid at 870 K are shown in Fig. 7. Both ring types were found in two possible geometries which are generally called ''boat'' and ''chair'' configurations, for obvious reasons. To allow a better comparison with theoretical and experimental work, we have calculated the average of the geometrical parameters of the different rings. This was done by averaging the interatomic distances and bond angles over the longest period during which the rings were present. The rings in the

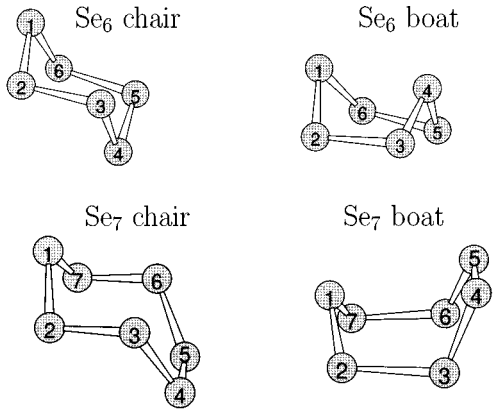

FIG. 7. The structures of Se_6 and Se_7 rings found in the simulation of ℓ-Se at 870 K in the chair and boat configurations.

liquid have no defined symmetry, and to facilitate the comparison with other calculations we have averaged the parameters in a way that allows direct comparison with the properties of isolated rings. The structural parameters obtained in this way are shown in Table VI where they are compared with the results of DFT-LDA calculations for isolated rings.[57]

TABLE VI. Structural parameters of the different types of rings found in ℓ-Se at 870 K. The values in the table represent the average value of the geometric parameters, taken over the lifetime of the rings. A hyphen means that the statistics are too poor to deduce meaningful averages. Also shown are results of DFT-LDA calculations on isolated Se_n rings from Ref. 57 as well as experimental results for the Se_6 rings found in monoclinic Se. For the definition of the atom numbering i, see Fig. 7. The distances r_{ij} are in Å and the bond angles $\Theta_i = \Theta_{jik}$ and dihedral angles $\gamma_{ij} = \gamma_{kijkl}$ in degrees.

		This work	DFT-LDA	Expt.
Se_6 chair	r_{ij}	2.42	2.35	2.34[a]
	Θ_i	102	101	101.3
	γ	75	76	76.2
Se_6 boat	$r_{12,16,34,45}$	2.43	2.31	
	$r_{23,56}$	2.48	2.52	
	$\Theta_{1,4}$	103	98	
	$\Theta_{2,3,5,6}$	101	107	
	$\gamma_{12,16,34,45}$	65	79	
	$\gamma_{23,56}$	~ 0	0	
Se_7 chair/boat	$r_{12,17}$	2.42/2.46	2.36/2.32	
	$r_{23,67}$	2.45/2.46	2.42/2.46	
	$r_{34,56}$	2.35/2.32	2.27/2.23	
	r_{45}	2.52/2.53	2.50/2.55	
	Θ_1	106/120	106/108	
	$\Theta_{2,7}$	101/99	101/100	
	$\Theta_{3,6}$	106/106	106/108	
	$\Theta_{4,5}$	105/108	105/103	
	$\gamma_{12,71}$	74/–	75/71	
	$\gamma_{23,67}$	106/–	110/44	
	$\gamma_{34,56}$	85/–	86/89	

[a]Reference 55.

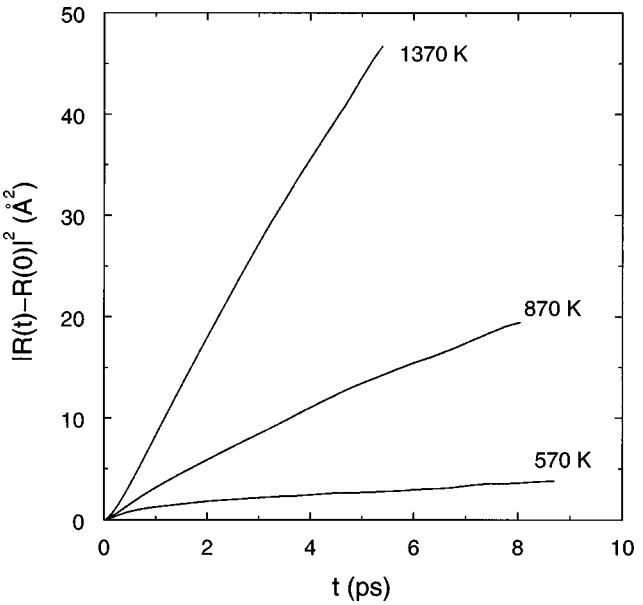

FIG. 8. The calculated mean-square displacement as a function of time in ℓ-Se at 570, 870, and 1370 K.

One sees from the table that the structural parameters found in the liquid are surprisingly close to those of isolated rings. The agreement is particularly good for the Se_6 and Se_7 rings in their chair configurations. We observe that the distances are systematically larger in the liquid, a fact that is attributable both to thermal expansion and to the contraction of the Se-Se bonds in isolated systems. The Se_6 chair configuration is also the building block of the rhombohedral crystalline phase,[55] and we have therefore included the experimental data, which are astonishingly close the DFT-LDA values of Ref. 57. To our knowledge, no experimental data have been published for the structure of Se_7 rings. In analogy to sulfur, for which a crystalline phase composed of S_7 rings is known,[58] it seems likely that Se_7 will be found in the chair structure [Fig. 7(d)]. This is indeed the ground-state geometry determined by Hohl *et al.*,[57] which our calculations reproduce very well. The boat configuration was only observed for a short time, and only approximate structural parameters could be calculated. The agreement with the data for the isolated ring is nevertheless satisfactory.

V. DYNAMICAL PROPERTIES

In this section we present and discuss results for the dynamical properties of ℓ-Se such as the diffusion, the bond lifetime, and the vibrational properties at different temperatures.

A. Self-diffusion constant

The simplest way to investigate atomic transport in liquids is to calculate the time-dependent mean-square displacement $\langle R^2(t)\rangle$, which is related to the self-diffusion constant D through the Einstein relation

$$\langle R^2(t)\rangle \rightarrow 6Dt + c \tag{6}$$

in the long-time limit $t \rightarrow \infty$. In Fig. 8 we show our results for the mean-square displacement for all three temperatures. At the lowest temperature the linear dependence of $\langle R^2(t)\rangle$ on t develops very slowly, and after 10 ps the atoms have on

TABLE VII. Self-diffusion constants (units of $\times 10^{-9} m^2/s$) of ℓ-Se at different temperatures as found in our simulations, compared to experimental data derived from inelastic neutron-scattering measurements; values in parentheses show the self-diffusion constant derived from the velocity autocorrelation function.

T (K)	This work	Expt.[a]	Expt.[b]
570	<0.5 (1.0)	0.4	0.2
870	3.5 (3.8)	1.9	22.0
1370	17.5 (17.0)	5.4	

[a]Reference 59.
[b]Reference 60.

average moved by less than the nearest-neighbor distance. We are therefore not able to give an accurate value for the diffusion constant at this temperature. For the other two temperatures $\langle R^2(t)\rangle$ is clearly linear for large t; at 870 K the atoms have on average moved by about twice the nearest-neighbor distance after 10 ps.

The self-diffusion constant was estimated via the Einstein relation [Eq. (6)] from a least-square fit to the mean-square displacement in the linear region. The results are reported in Table VII, where they are compared with experimental data obtained from two different quasielastic neutron-scattering experiments.[59,60]

It is important to note that both sets of experimental measurements were done only over a very limited temperature range. Those of Axmann *et al.*[59] covered the range 523–723 K, while the results of Phillips *et al.*[60] covered the even smaller range ~500–600 K. However, both experimental groups report an activation energy E_D obtained by fitting an Arrhenius form:

$$D = D_0 \exp(-E_D/k_B T) \tag{7}$$

to their data. The values of E_D deduced by Axmann *et al.* and by Phillips *et al.* are 0.21 and 0.7 eV, respectively. The ''experimental'' values given in Table VII for 870 K are obtained from the Arrhenius equation using these E_D values. Given the very different activation energies, the extrapolated values are necessarily different. Since Axmann *et al.* covered a larger temperature range, we believe their values should be preferred. The most that can be said at present is that our calculated values of D are in semiquantitative agreement with experiment. The activation energy estimated from our results for D by fitting to the Arrhenius form is 0.29 eV, which is in reasonable agreement with the value of Axmann *et al.*, but not with that of Phillips *et al.*

B. Velocity autocorrelation function and spectral density

More detailed information about the single-particle dynamics can be obtained by studying the velocity autocorrelation function (VACF) $Z(t)$ defined as[61]

$$Z(t) = \frac{\langle \mathbf{v}_i(0)\cdot\mathbf{v}_i(t)\rangle}{\langle \mathbf{v}_i(0)\cdot\mathbf{v}_i(0)\rangle}, \tag{8}$$

where $\mathbf{v}_i(t)$ is the velocity of particle i and $\langle\rangle$ denotes an average over particles and over time origins. The corresponding spectral density $\hat{Z}(\omega)$ is given by

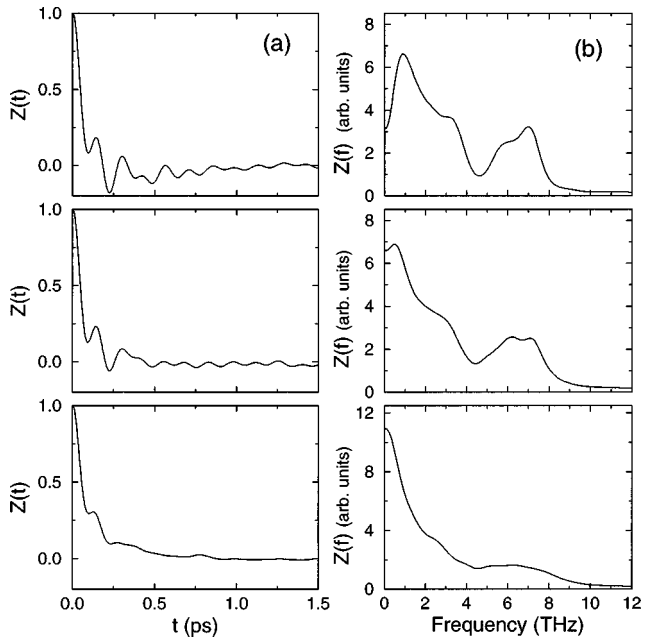

FIG. 9. The velocity autocorrelation function $Z(t)$ (a) of ℓ-Se at 570 (top), 870 (middle), and 1370 K (bottom) and the corresponding spectral density $\hat{Z}(f)$ (b).

$$\hat{Z}(\omega) = \int_0^\infty Z(t)\cos(\omega t)\,dt. \tag{9}$$

Because $Z(t)$ shows significant oscillations at long time, we introduced a window function to filter out the termination ripples that would occur in $\hat{Z}(\omega)$ if $Z(t)$ were artificially truncated. We used a Welsh-type window function,[62] with a typical window length of 2.0 ps, which gives a frequency resolution of approximately 0.4 THz.

The VACF and the corresponding spectral densities are shown in Fig. 9 for all three temperatures. For a purely Brownian motion the VACF would decay monotonically. In liquid Se oscillations are superimposed on this diffusive background. These oscillations are much stronger at lower temperature, and decay very slowly at 570 K.

The spectral density $\hat{Z}(\omega)$ at 570 K reveals four well-defined features at frequencies of 0.9, 3.2, 6.3, and 7.3 THz and the zero-frequency value $\hat{Z}(0)$ is rather small, so that the dynamics is dominated by vibrational rather than diffusive motion. The four features are considerably broader, though still clearly visible at 870 K. At 1370 K vibrational modes are reduced to a broad shoulder at high frequencies, and the dominant feature is the zero-frequency peak associated with diffusion. We note in passing that we can check our values for the self-diffusion constants using the relation

$$D = \frac{k_B T}{M}\int_0^\infty Z(t)\,dt = \frac{k_B T}{M}\hat{Z}(0). \tag{10}$$

The values obtained in this way agree satisfactorily with those discussed in the previous subsection (see Table VII). The largest discrepancies are found for the low temperature, and we have already mentioned that there are statistical problems in calculating the low-temperature value of D.

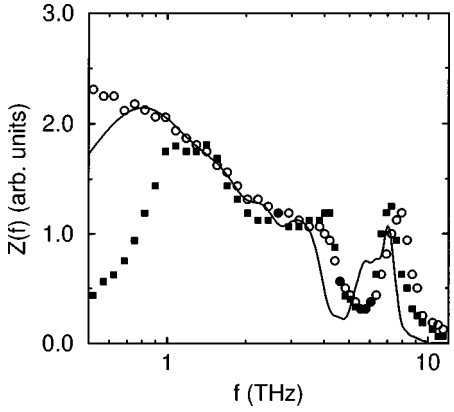

FIG. 10. The spectral density of the velocity autocorrelation function $\hat{Z}(f)$ of ℓ-Se at 570 K compared to frequency-dependent scattering intensity from Ref. 60 measured at 470 K for the undercooled liquid (open circles) and polycrystal (filled squares).

The vibrational properties of a-Se and ℓ-Se have been studied using inelastic neutron scattering by Phillips *et al.*[60] and in Fig. 10 we compare our spectral density with their frequency-dependent scattering intensity. The close relation between the theoretical and experimental results is very gratifying. Both the positions and the intensities of the main peaks are in satisfactory agreement. Phillips *et al.* assigned their three main peaks to bond torsion, bending and stretching, in order of increasing frequency.

The only qualitative difference between theory and experiment is the splitting of the high-frequency peak seen in our simulations but not in the experiment. However, this may not be significant, because our spectral density does not correspond exactly to what is measured in the experiments.

C. Bond lifetime

Except for the low diffusion constant at 570 K, our values of D are similar to those found in liquid metals. This raises the question of how the atoms manage to diffuse so fast in spite of the well-defined chain structure. One can imagine two pictures of how the atoms diffuse. At one extreme, it is conceivable (though unlikely) that diffusion occurs by motion of whole chain fragments, and does not depend on the breaking of bonds. At the other extreme, one might imagine that diffusion occurs solely by hopping of single atoms, so that it depends entirely on the breaking of bonds. Most likely, the true picture lies somewhere between these extremes. To give more insight, we have examined the lifetime of bonds.

We start by introducing the probability $P_b(t)$ of finding two atoms bonded together at time t, given that they were bonded at $t=0$. This function is defined by

$$P_b(t)=\langle f_{ij}^b(0) f_{ij}^b(t)\rangle / \langle f_{ij}^b(0) f_{ij}^b(0)\rangle, \tag{11}$$

where $f_{ij}^b(t)$ is a dynamical variable which is unity if atoms i, j are bonded at time t and is zero otherwise:

$$f_{ij}^b(t)=\theta(r_c-r_{ij}(t)), \tag{12}$$

with $\theta(r)$ the Heaviside function. The angular brackets in Eq. (11) represent averaging over atom pairs and time origins. As usual, the cutoff distance r_c distinguishes between bonded and nonbonded atoms, and we take this cutoff to be the first-minimum distance $r_{\min}$.

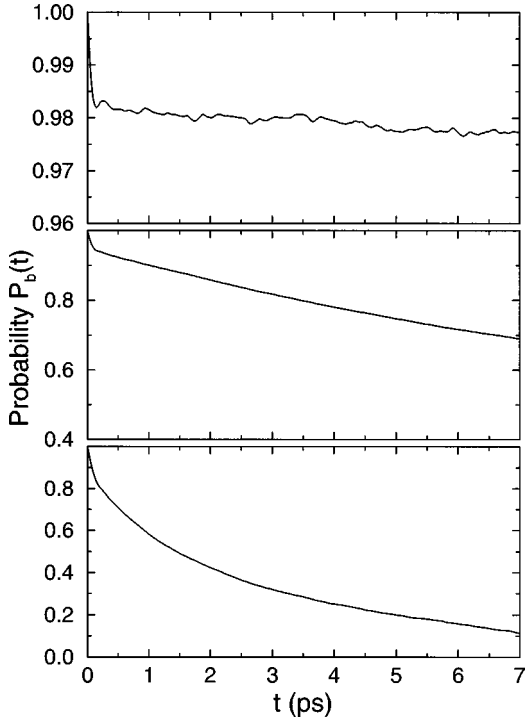

FIG. 11. The bonding probability function $P_b(t)$ for pairs of atoms in ℓ-Se at 570 (top), 870 (middle), and 1370 K (bottom).

In Fig. 11 we plot $P_b(t)$ for all three temperatures as calculated from our simulations. The general characteristics of $P_b(t)$ are the same at all three temperatures. Within 0.1 ps P_b drops significantly, and then it decreases monotonically with time. We believe that the initial drop of P_b is caused by thermal vibrations. The subsequent decay of P_b is very slow at 570 K, but much faster at the two higher temperatures.

The bond lifetime τ is conveniently defined as

$$\tau=\lim_{t\to\infty}\int_0^t P_b(t')dt'. \tag{13}$$

Two technical points should be noted. The first is that in a finite system P_b tends to the value $\overline{N_c}/N$ as $t\to\infty$ (N is the number of atoms in the cell, $\overline{N_c}$ is the average coordination number), because there is always a finite probability of finding any two atoms bonded together. This asymptotic constant should be subtracted from P_b before the time integral is performed. The second point is that in practice P_b is known only over a finite time, so that a procedure is needed for taking the $t\to\infty$ limit. To deal with this second point, we assume that $P_b(t)$ decays as $\exp(-t/\tau)$, and we obtain τ from a fit of the curves shown in Fig. 11. The values for τ estimated in this way are given in Table VIII. Because of the very slow decay of $P_b(t)$ at 570 K, our value for τ at this temperature is only a rough estimate. The lifetimes of 20 and 3 ps obtained at 870 and 1370 K should, however, be reliable. Interestingly, the 870 K value is close to the value of 15 ps deduced by Axmann *et al.*[59] from their neutron-scattering measurements.

TABLE VIII. Estimated bond lifetimes τ in ℓ-Se at different temperatures. We also show r.m.s. diffusive $\langle R^2(\tau)\rangle^{1/2}$ after time τ (see text).

T (K)	τ (ps)	$\langle R^2(\tau)\rangle^{1/2}$ (Å)
570	>200	
870	20	6.5
1370	3	5.5

If we combine these results with our calculated diffusion constants, we can estimate the average distance which an atom diffuses in a bond lifetime. We calculate this as the root-mean-square value $(6D\tau)^{1/2}$ expected from the Einstein relation [Eq. (6)]. The values obtained are ~ 5 Å at both 870 and 1370 K (see Table VIII). Since this is roughly twice the nearest-neighbor distance, we conclude that diffusion should not be considered to occur *solely* by jumping of isolated atoms. It appears that motion of atoms due to deformation of chain fragments without bond breaking gives a significant contribution to diffusion.

VI. ELECTRONIC DENSITY OF STATES

We present here our simulation results for the total electronic density of states (DOS). The local DOS on atoms of different coordination number is also of interest, but will not be examined here, since it will be more appropriate to discuss it in our separate report on defects in ℓ-Se.[29] Our DOS results were obtained by sampling during each FPMD run (i.e., only the Γ point was used). It should be noted that the DOS is calculated only over the energy range covered by partially occupied states in our simulations, i.e., from the lowest state up to an energy of approximately ~ 2 eV above the Fermi energy. This means that our DOS curves are artificially truncated at this energy.

The calculated DOS at 570, 870, and 1370 K are shown in Fig. 12. They all have the same general shape, and closely resemble the calculated DOS for t-Se.[16] The two main features in the DOS centered at -13 eV and -2 eV derive from Se 4s and 4p states. The structure of these features reflects the strong intrachain covalent bonding that persists in the liquid. The 4s feature shows splitting into bonding and antibonding states, while the 4p feature contains peaks due to bonding ($pp\sigma$), nonbonding ($pp\pi$), and antibonding ($pp\sigma^*$) states. The Fermi level falls between $pp\pi$ and $pp\sigma^*$ states, so that the bonding in the chains is due to the fact that $pp\sigma$ states are full and $pp\sigma^*$ states are empty.

Experimentally, both t-Se and ℓ-Se have a sizeable band gap E_g between the nonbonding and antibonding 4p states: in t-Se, $E_g = 2.0$ eV, while in the liquid E_g decreases from ~ 1.9 eV at 473 K to ~ 1.0 eV at 1173 K.[63] Our DFT calculations seriously underestimate E_g, since we find a gap of about zero at 573 K, and no gap at all at higher temperatures. The gap calculated in t-Se is ~ 1.0 eV.[16] This underestimation of band gaps is a very well-known property of DFT calculations. It is also well recognized that a direct comparison with experiment is not justified, since the theoretical energies we are comparing are Kohn-Sham single-particle energies, which are distinct from the quasiparticle energies measured in optical absorption experiments. The disagreement is therefore not an indication of any deficiency in the DFT calculations: it simply indicates that we are not comparing like with like. However, given the importance of the band gap in ℓ-Se, it would clearly be desirable to calculate quasiparticle energies, and we hope to return to this question in a future paper.

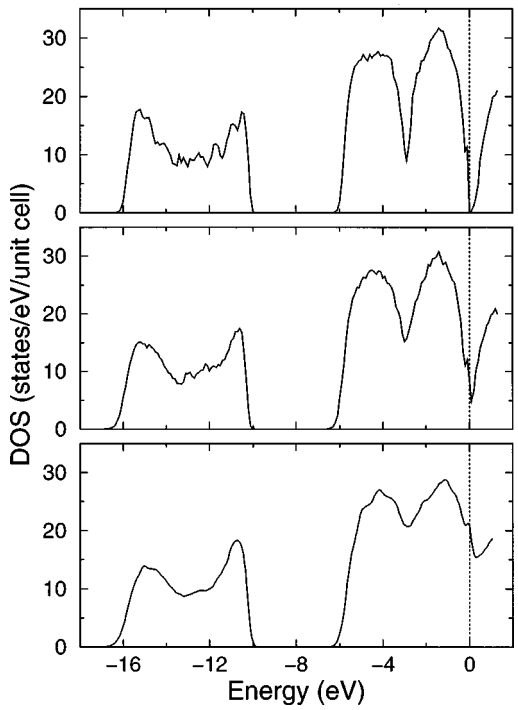

FIG. 12. The total electronic density of states in ℓ-Se at 570 (top), 870 (middle), and 1370 K (bottom). The dotted line at zero energy represents the Fermi level. The curves have been convoluted with a Gaussian of a width of 0.1 eV.

VII. CONCLUSION

An important conclusion from this first-principles simulation work on ℓ-Se is that LDA has serious difficulties, which are reduced by GGA. The main difficulty is that LDA grossly underestimates the equilibrium volume, this underestimation being $\sim 15\%$ in the solid. The consequence is that if one simulates the liquid at the experimental density, the system is at a negative pressure, and is unstable with respect to long-wavelength density fluctuations. The GGA gives an equilibrium volume which is almost correct, and this eliminates the problem.

We have shown that the structure factor and pair-correlation function calculated with GGA are in fairly close agreement with experiment over the whole temperature range 570–1370 K, and we therefore expect the three-dimensional structure of our simulated Se to give an accurate picture of the real liquid. The average coordination of the atoms remains close to 2 up to 1370 K, though the fraction of atoms having lower or higher coordinations increases markedly with increasing T. In agreement with earlier work, we find that ℓ-Se consists mainly of chain fragments. The geometrical method we use gives a chain length decreasing from 25 to 5 as T goes from 570 to 1370 K, but we have cautioned against a naive comparison of these values with previous

estimates, because of the problem of arbitrariness in defining chain length. In contrast to the FPMD work of Hohl *et al.*,[14] we find a significant concentration of rings (especially Se_7 rings) at 870 K, but not at low or high temperatures. The bond-angle distribution has a pronounced peak at 104° over the whole temperature range, indicating that the short-range order in the liquid remains very similar to that in the solid. The dihedral-angle distribution shows a maximum around 90° at lower temperatures, but this disappears at high temperatures.

Our calculated values of the self-diffusion constants D at 570 and 870 K are in semiquantitative agreement with experimental values, though the value at 570 K is too small to calculate accurately. At 870 K and above, D has the same order of magnitude as for simple liquids like Na. Our results for the bond lifetime suggest that the diffusion of Se atoms occurs partly by bond-breaking jumps of individual atoms and partly by collective motion of chains. The calculated single-particle vibrational spectrum corresponds closely with the neutron-scattering spectrum reported by Phillips *et al.*, with all the characteristic vibrational frequencies measured experimentally being reproduced almost quantitatively in the simulations.

The calculated electronic density of states of the liquid strongly resembles that calculated for t-Se, indicating that the electronic structure is not much affected by melting. However, there is a difficulty in making a detailed comparison with experiment, since the Kohn-Sham energies we calculate show at best only a very small band gap, in contrast to experimental quasiparticle energies which show a band gap of at least 1.0 eV in the liquid.

An important question not discussed in this paper concerns the geometry and electronic structure of defects in the liquid. This question will be examined in depth in a separate paper.[29]

ACKNOWLEDGMENTS

This work was supported by EPSRC Grants No. GR/L08946 and GR/L38592. An allocation of time on the Fujitsu VPX 240 machine at Manchester Computer Center under EPSRC Grant No. GR/69974 is gratefully acknowledged. F.K. acknowledges financial support from ORS.

*Present address: Institut für Theoretische Physik, Technische Universität Wien, Wiedner Hauptstr. 8-10/136, A-1040 Wien, Austria.

[1] H. Hoshino, R. W. Schmutzler, W. W. Warren, and F. Hensel, Ber. Bunsenges. Phys. Chem. **80**, 27 (1976).
[2] R. O. Jones and O. Gunnarsson, Rev. Mod. Phys. **61**, 689 (1989).
[3] R. Car and M. Parrinello, Phys. Rev. Lett. **55**, 2471 (1985).
[4] I. Štich, R. Car, and M. Parrinello, Phys. Rev. B **44**, 11 092 (1991), and references therein.
[5] G. Kresse and J. Hafner, Phys. Rev. B **47**, RC558 (1993).
[6] G. Kresse and J. Hafner, Phys. Rev. B **49**, 14 251 (1994).
[7] G. Kresse and J. Hafner, Phys. Rev. B **48**, 13 115 (1993).
[8] P. E. Blöchl and M. Parrinello, Phys. Rev. B **45**, 9413 (1992).
[9] G. Kresse, J. Non-Cryst. Solids **192+193**, 222 (1995).
[10] J. M. Holender, M. J. Gillan, M. C. Payne, and A. D. Simpson, Phys. Rev. B **52**, 967 (1995).
[11] G. Kresse and J. Hafner, Phys. Rev. B **55**, 7539 (1997).
[12] J. M. Holender and M. J. Gillan, Phys. Rev. B **53**, 4399 (1996).
[13] F. Kirchhoff, J. M. Holender, and M. J. Gillan, Phys. Rev. B **54**, 190 (1996).
[14] D. Hohl and R. O. Jones, Phys. Rev. B **43**, 3856 (1991).
[15] A. Dal Corso and R. Resta, Phys. Rev. B **50**, 4327 (1994).
[16] G. Kresse, J. Furthmüller, and J. Hafner, Phys. Rev. B **50**, 13 181 (1994).
[17] Y. Wang and J. P. Perdew, Phys. Rev. B **44**, 13 298 (1991).
[18] K. Suzuki, Ber. Bunsenges. Phys. Chem. **80**, 689 (1976).
[19] M. Misawa and K. Suzuki, Trans. Jpn. Inst. Met. **18**, 427 (1977).
[20] R. Bellissent and G. Tourand, J. Non-Cryst. Solids **35–36**, 1221 (1980).
[21] M. Edeling and W. Freyland, Ber. Bunsenges. Phys. Chem. **85**, 1049 (1981).
[22] K. Tamura and S. Hosokawa, Ber. Bunsenges. Phys. Chem. **96**, 681 (1992).
[23] K. Tamura, M. Inui, M. Yao, H. Endo, S. Hosokawa, H. Hoshino, Y. Katayama, and K. Maruyama, J. Phys.: Condens. Matter **3**, 7495 (1991).
[24] M. Misawa and K. Suzuki, J. Phys. Soc. Jpn. **44**, 1612 (1978).
[25] A. Eisenberg and A. V. Tobolsky, J. Polym. Sci. **46**, 19 (1960).
[26] G. Lucovsky, in *The Physics of Selenium and Tellurium*, edited by E. Gerlach and P. Grosse (Springer, Berlin, 1979), p. 178.
[27] J. C. Perron, J. Rabit, and J. F. Rialland, Philos. Mag. B **46**, 321 (1982).
[28] W. W. Warren and R. Dupree, Phys. Rev. B **22**, 2257 (1980).
[29] G. Kresse, F. Kirchhoff and M. J. Gillan (unpublished).
[30] F. Kirchhoff, M. J. Gillan, J. M. Holender, G. Kresse, and J. Hafner, J. Phys.: Condens. Matter **8**, 9353 (1996).
[31] M. C. Payne, M. P. Teter, D. C. Allan, T. A. Arias, and J. D. Joannopoulos, Rev. Mod. Phys. **64**, 1045 (1992).
[32] G. Kresse and J. Furthmüller, Comput. Mater. Sci. **6**, 15 (1996).
[33] G. Kresse and J. Furthmüller, Phys. Rev. B **54**, 11 169 (1996).
[34] P. Pulay, Chem. Phys. Lett. **73**, 393 (1980).
[35] N. D. Mermin, Phys. Rev. **137**, 1441 (1965).
[36] M. J. Gillan, J. Phys.: Condens. Matter **1**, 689 (19180).
[37] D. Vanderbilt, Phys. Rev. B **41**, 7892 (1990).
[38] G. Kresse and J. Hafner, J. Phys.: Condens. Matter **6**, 8245 (1994).
[39] A. M. Rappe, K. M. Rabe, E. Kaxiras, and J. D. Joannopoulos, Phys. Rev. B **41**, 1227 (1990).
[40] S. G. Louie, S. Froyen, and M. L. Cohen, Phys. Rev. B **26**, 1738 (1982).
[41] We use the parametrization presented by J. P. Perdew and A. Zunger, Phys. Rev. B **23**, 5048 (1981).
[42] S. Nosé, J. Chem. Phys. **81**, 511 (1984).
[43] Y. Akahama, M. Kobayashi, and H. Kawamura, Phys. Rev. B **47**, 20 (1993).
[44] H. Akbarzadeh, S. J. Clark, and G. J. Ackland, J. Phys.: Condens. Matter **5**, 8065 (1993).
[45] D. Vanderbilt and J. D. Joannopoulos, Phys. Rev. B **27**, 6296 (1983); **27**, 6302 (1983); **27**, 6311 (1983).
[46] W. Richter, in *The Physics of Selenium and Tellurium*, edited by E. Gerlach and P. Grosse (Springer, Berlin, 1979), p. 36.
[47] R. Zallen and G. Lucovsky, in *The Physics of Selenium and Tellurium*, edited by C. Cooper (Pergamon, New York, 1969), Chap. 4.
[48] S. Hosokawa and K. Tamura, J. Non-Cryst. Solids **117/118**, 52 (1990).

[49] J. Thurn and J. Ruska, J. Non-Cryst. Solids **22**, 331 (1972).
[50] N. E. Cusack, *The Physics of Structurally Disordered Matter* (Adam Hilger, Bristol, 1987).
[51] R. Steudel, Angew. Chem. Int. Ed. Engl. **14**, 655 (1975).
[52] D. Hohl, R. O. Jones, R. Car, and M. Parrinello, J. Chem. Phys. **89**, 6823 (1988).
[53] C. Bichara, A. Pellegatti, and J.-P. Gaspard, Phys. Rev. B **49**, 6581 (1994).
[54] P. Cherin and P. Unger, Acta Crystallogr., Sect. B: Struct. Crystallogr. Cryst. Chem. **28**, 313 (1972).
[55] Y. Myamoto, Jpn. J. Appl. Phys. **19**, 1813 (1980).
[56] R. Steudel and E.-M. Strauss, Adv. Inorg. Chem. Radiochem. **28**, 135 (1984).
[57] D. Hohl, R. O. Jones, R. Car, and M. Parrinello, Chem. Phys. Lett. **139**, 540 (1987).
[58] R. Steudel, Z. Anorg. Allg. Chem. **478**, 139 (1981).
[59] A. Axmann, W. Gissler, A. Kollmar, and T. Springer, Discuss. Faraday Soc. **50**, 74 (1970).
[60] W. A. Phillips, U. Buchenau, N. Nücker, A.-J. Dianoux, and W. Petry, Phys. Rev. Lett. **63**, 2381 (1989).
[61] J.-P. Hansen and I. R. McDonald, *Theory of Simple Liquids* (Academic, London, 1986), p. 199.
[62] W. H. Press, B. P. Flannery, S. A. Teukolsky, and W. T. Vetterling, *Numerical Recipes* (Cambridge University Press, New York, 1986).
[63] S. Hosokawa and K. Tamura, J. Non-Cryst. Solids **117/118**, 489 (1990).